PCCP

Incorporation of Single Rhodium Atoms to Ceria Surface for Promotion of Catalytic Performance in Partial Oxidation of Methane

Journal:	*Physical Chemistry Chemical Physics*
Manuscript ID	CP-ART-07-2022-003216.R1
Article Type:	Paper
Date Submitted by the Author:	03-Oct-2022
Complete List of Authors:	Opalade, Adedamola; University of Kansas College of Liberal Arts and Sciences, Chemistry Tang, Yu; University of Kansas School of Engineering, Chemical and Petroleum Engineering Tao, Franklin; University of Kansas School of Engineering, Chemical and Petroleum Engineering

ARTICLE

Integrated In-situ Spectroscopy Studies on Syngas Production from Partial Oxidation of Methane Catalyzed by Atomically Dispersed Rhodium Cations on Ceria

Received 00th January 20xx,
Accepted 00th January 20xx

DOI: 10.1039/x0xx00000x

Adedamola A. Opalade, [a,b] Yu Tang, *[a] and Franklin (Feng) Tao *[a]

Catalytic reforming of methane to produce syngas is an important prodcution of value-added chemicals. The conventional reforming catalyst relies on supported nickel nanoparticles. Herein, we investigated a singly dispersed Rh cations anchored on CeO_2 catalyst (Rh_1/CeO_2) for high activity and selectivity towards production of syngas through partial oxidation of methane (POM) in the temperature range of 600-700 °C. The yields of H_2 and CO at 700 °C are 83% and 91%, respectively. The anchored Rh_1 atoms on CeO_2 of Rh_1/CeO_2 are at cationic state and on average each Rh_1 atom coordinates with 4-5 surface lattice oxygen atoms of CeO_2 under the POM condition. Compared to the inert CeO_2 for POM, the incorporation of single-atom sites, Rh_1 modifies electronic state of oxygen atoms proximal to the Rh_1 atoms and thus triggers catalytic activity of CeO_2. The high activity of single-atom catalyst Rh_1/CeO_2 suggests that an incorporation of single atoms of transition metals to surface of a reducible oxide can modulate electronic state of its proximal anions of the oxide support toward forming an electronic state favorable for selective formation of ideal products.

1. Introduction

Syngas, a mixture of CO and H_2 is one of the most important raw materials of chemical industries for syntheses of a great number of important intermediate compounds for production of value-added chemicals through Fischer-Tropsch synthesis (FTS).[1-5] Syngas with a stoichiometric ratio of H_2/CO at 2 is optimal for the synthesis of methanol.[6] Steam reforming of methane (SRM),[7] which is the commonly used process for reforming methane, produces syngas with a stoichiometric ratio of H_2/CO to be 3/1; the main limitation of SRM is its thermodynamics in terms of being a highly endothermic reaction, requiring a quite high temperature for achieving an ideal conversion of CH_4.[8] Carbon dioxide reforming of methane, also called dry reforming of methane (DRM) produces a syngas with a stoichiometric ratio of H_2/CO at 1/1; a drawback of DRM is the simultaneous occurrence of the reverse water gas shift (RWGS) reaction,[9, 10] which produces syngas with H_2/CO ratio lower than 1.0. Syngas with a low H_2/CO ratio is not favorable for production of light hydrocarbons in a downstream FTS process upon DRM. In addition, DRM is more endothermic than SRM and thus requests a higher catalysis temperature to achieve the same conversion of CH_4 as SRM. Compared to SRM and DRM, partial oxidation of methane (POM) is attractive;[11, 12] it circumvents the request of high temperature since it is essentially exothermic and it can produce syngas with an ideal ratio of H_2/CO at 2/1, a favorable composition for production of significant intermediate compounds including methanol, one of the most important raw materials of chemical and energy industries.[6, 13]

CH_4 has the highest H/C ratio (4) among all hydrocarbons. It is difficult to activate its C–H bonds because the sp^3 hybridization of the atomic orbitals of carbon atom makes the C–H bonds quite strong with a bond energy as high as 439 kJ/mol.[14, 15] The rate-determining step in methane activation is the cleavage of the first C–H bond typically or the second C-H bond in some cases.[16-20] In general, methane is readily activated by Group 8, 9, and 10 transition metals.[21] Among these transition metal catalysts, catalysts of supported noble metals were extensively studied in literature.[10-12] Noble metals are prohibitively expensive due to their low abundance in earth. Therefore, development of catalysts toward reducing use of noble metals while promoting catalytic activity and selectivity has been of prime significance in designing efficient POM catalysts.[22-25] Much attention has been made to downsizing metal nanoparticles as the downsizing approach has demonstrated its promotion effect to catalytic performance through modification of coordinative environment of active metal sites,[26] quantum size effect where confinement of electrons leads to widening of the HOMO-LUMO gap,[27, 28] metal-support interaction where metal-support chemical bonds become stronger,[29, 30] and cluster configuration where the specific arrangement and limited number of metal atoms in a cluster results in a change in the physicochemical properties of the catalyst.[31, 32] In the last decade, incorporation of single-atom sites has been an important approach in rationally designing a catalyst with high activity and selectivity.[33, 34] Compared to variation of size of metal nanoparticle, single dispersion of each atom of a noble metal element is expected to tune electronic

[a] Department of Chemical and Petroleum Engineering, University of Kansas, KS 66045, USA. Email: tangyu.zju@gmail.com (YT) and franklin.tao.2017@gmail.com (FT).
[b] Department of Chemistry, University of Kansas, KS 66045, USA

state of catalytic site significantly, providing a practical channel to achieve catalysis with high activity and selectivity.[20, 33]

In this work, Rh was chose as noble metal for POM. The catalyst consisting of CeO_2 nanorods with singly dispersed Rh_1 atoms was prepared for developing a POM catalyst toward having high activity and selectivity. CeO_2 nanorods were synthesized by the hydrothermal method as reported in the literature.[35] Then, Rh_1/CeO_2 was prepared by a deposition-precipitation method for anchoring Rh atoms onto the surface of the prepared CeO_2 nanorods. *In-situ* X-ray absorption spectroscopy (XAS) including X-ray Absorption Near Edge Spectroscopy (XANES) and Extended X-ray absorption fine structure (EXAFS), and ambient pressure X-ray photoelectron spectroscopy (AP-XPS) were used to study the atomic scale chemical and coordination environments of Rh atoms of 0.20wt%Rh/CeO_2 during catalysis. As these characterizations confirmed the single dispersion of Rh atoms. Evaluation of catalytic performance showed that the CeO_2 with supported single atom sites is highly active for POM with high selectivity for production of syngas instead pure CeO_2 is insert for this reaction. The integrated analysis of the spectra from these spectroscopies aided the interpretation of the outstanding catalytic performance of CeO_2 with supported single atom sites.

2. Experimental method

2.1 Synthesis methods

Hydrothermal Synthesis of CeO_2 nanorods. The CeO_2 nanorods were prepared by a revised hydrothermal method.[35] 6.0 M NaOH solution was prepared by dissolving 16.8 g of NaOH in 70 mL H_2O contained in the Teflon lining of an autoclave. 0.204 g of $Ce(NO_3)_3 \cdot 6H_2O$ was dissolved in 10 mL H_2O. The $Ce(NO_3)_3 \cdot 6H_2O$ resulting solution was added dropwise to the prepared NaOH solution under vigorous stirring until complete addition. Then, the Teflon lining was covered, and the mixture was stirred at 1150 rpm for 1 hour. The Teflon lining was placed into a steel jacket of the autoclave and then the autoclave was closed tightly and placed in an oven at 120°C for 24 hours. After 24 hours, the resulting mixture was centrifuged to obtain a solid slurry. The slurry was repeatedly washed with deionized H_2O and centrifuged 7 times till a pH of 7.5 was obtained; then, the slurry was dried in an oven in air at 80°C for 24 hours. The dried sample was pulverized in an agate mortar and pestle and calcined at 450°C for 2 hours, giving the yellowish CeO_2 nanorods powder.

Synthesis of 0.20wt% Rh_1/CeO_2. The nominal concentration of Rh in the Rh_1/CeO_2 catalyst is 0.20wt%. Rh_1/CeO_2 was made by deposition-precipitation method. In a typical preparation, 2.925 g of CeO_2 was dispersed in 80 mL of deionized (DI) H_2O. The mixture was stirred using a magnetic stirrer at 650 rpm to aid the dispersion of the CeO_2 nanopowder in the solution. The mixture was sonicated at intervals to ensure the CeO_2 nanopowder evenly dispersed in the water. After the CeO_2 was evenly dispersed, the mixture was stirred continuously for another hour. $Rh(NO_3)_3 \cdot$ solution was prepared by dissolving 16.25 mg of $Rh(NO_3)_3.xH_2O$ in 30 mL of DI H_2O. This $Rh(NO_3)_3$ solution was transferred into a 30 mL syringe. It was added to the solution of well dispersed CeO_2 nanorods under stirring (800 rpm) at a flow rate of 0.1 mL/min in a manner of dropwise with the aid of a needle. Then, the mixture was sealed with paraffin film to prevent evaporation and the mixture was stirred continuously for 24 hours. After 24 hours, the mixture was centrifuged at 4500 rpm for 5 minutes to obtain the solid pellet. The pellet was dried in air at 60°C for 24 hours, pulverized and calcined at 350°C for 2 hours to obtain the 0.20wt% Rh/CeO_2. The calculation temperature is significant for forming a specific coordination environment of Rh_1 atoms.

2.2 Catalyst characterization.

The actual loading of Rh element of the Rh_1/CeO_2 catalyst was determined by Inductively Coupled Plasma Optical Emission Spectroscopy (ICP-AES) using the Horiba Jobin Yvon JY 2000 ICP-AES Spectrometer.

Crystallographic diffraction pattern of the 0.20% Rh/CeO_2 catalyst was performed using X-ray diffractometer with a Mo Kα (λ = 0.71073 Å) X-ray source. The size, morphology and lattice spacing of the 0.20% Rh/CeO_2 catalyst after reaction was studied with transmission electron microscope (JOEL JEM 2100F) operating at an accelerating voltage of 200 kV housed in the Petersen Institute of Nanoscience and Engineering Nanofabrication and Characterization Facility of the University of Pittsburgh. Analysis of the images were performed using the Digital Micrograph Software (Gatan, Inc.).

The pulsed CO chemisorption was performed on a Micrometric 3Flex surface analyser. 100 mg of the catalyst was heated at 200°C for 2 hours in 5% H_2/N_2 flow. After cooling to 50°C, the sample was exposed to different gas flows in the following ordering: i.) flow helium gas for 5 minutes, ii) flow oxygen gas for 5 minutes, iii) flow CO_2 gas for 10 minutes, iv) flow N_2 gas for 20 minutes, and v) finally flow H_2 gas for 5 minutes. A key step in the CO chemisorption measurement is the pre-injection of CO_2 for passivating the CeO_2 surface of 0.20wt%Rh/CeO_2 by forming carbonates on CeO_2; If this step is skipped, the dispersion of metal atoms on surface of the catalyst could largely over-estimated since CO can be adsorbed on the bare CeO_2 surface although only these CO molecules chemisorbed on Rh atoms should be counted in the measurement of dispersion of Rh atoms. After the above five steps of gas injections, CO was pulsed into the sample container every minute until the CO chemisorption onto the catalyst was saturated.

In situ characterization of surface of the 0.20wt% Rh/CeO_2 during catalysis was performed with an assembled commercial Ambient Pressure X-ray Photoelectron Spectrometer (AP-XPS).[36] This AP-XPS uses a monochromated Al Kα X-rays source to generate photoelectrons. The catalyst particles were loaded onto surface of a roughened gold foil by drop casting and the foil was affixed onto a sample holder in the reaction cell of the AP-XPS system. Then, the mixture of 0.6 Torr of methane and 0.3 Torr of O_2 was flowing through the reaction cell installed in the AP-XPS. Rh*3d*, Ce*3d* and O*1s* spectra were collected at 600°C and 650°C when the mixture of CH_4 and O_2 was flowing through the catalyst surface. The XPS data were analyzed and

deconvoluted with CasaXPS software. Peak positions of Rh 3d, O 1s, and Ce 3d were calibrated with the isolated u''' peak of Ce *3d* at 916.9 eV.[37, 38]

The diffuse reflectance infrared Fourier transform spectroscopy (DRIFTS) was performed on the CeO_2 nanorods and 0.20wt%Rh_1/CeO_2 using an Agilent Cary 670 FTIR equipped with a linearized Mercury-Cadmium-Telluride (MCT) detector, a Harrick diffuse reflectance accessory, and a Praying Mantis high-temperature reaction chamber. The reaction chamber was equipped with a KBr dome.

X-ray absorption spectroscopy (XAS) studies including X-ray Absorption Near Edge Spectroscopy (XANES) and Extended X-ray absorption fine structure (EXAFS) was performed at beam line 2-2 of Stanford Synchrotron Radiation Light Source (SSRL). The incident beam was tuned by a set of Si (220) double crystal monochromator. The absorption spectrum was collected with a Ge multichannel detector under fluorescence mode. XAS of the Rh K edge was recorded simultaneously with a Rh reference foil to calibrate each sample. The XAS data were processed and fitted with Athena and Artemis software program, respectively.[39] The coordination numbers were determined by fixing the amplitude reduction factor (S_o^2) value, which was obtained by fitting the reference Rh foil. XANES and EXAFS were performed under in situ study model. At end station of this beamline, the catalyst was loaded to a reaction cell[40, 41] where a mixture of CH_4 and O_2 with a flow rate of 25 ml/min and molar ratio of CH_4 to O_2 at 2/1 flew through the catalyst bed and was heat to a catalysis temperature and then was maintained at the temperatures for 0.5-1 hr for collection XAS data for XANES analysis. They were used for identification of oxidation state of the Rh atoms during catalysis. Then, the catalyst was cooled to 100°C -150°C or so when the mixture of reactants was still flowing through the catalyst bed. Data of XAS was collected at a temperature between 100°C-150°C in the flowing mixture of reactants, EXAFS studies; these data were used for generation of r-space spectrum of EXAFS which was fit for uncovering coordination environment of Rh atoms.

2.3 Evaluation of Catalytic Performance of Catalyst and Kinetic Studies.

Catalytic performance of the 0.20wt%Rh/CeO_2 and pure CeO_2 was measured in a fixed bed reactor. In a typical measurement, 30 mg of 0.20wt%Rh/CeO_2 or pure CeO_2 was mixed with 300 mg of quartz sand and then loaded in a quartz tube reactor. A gas mixture of 25 mL 10% CH_4/Ar and 25 mL 5% O_2 was introduced into the reactor. Catalysis temperature was measured with a K-type thermocouple inserted in the catalyst bed. The catalysis temperature was controlled using a proportional-integral-derivative (PID) temperature controller. Conversion of CH_4 was measured in the temperature range of 300°C-700°C with an increment of 50°C every 40 minutes. The reactant and product of this process were monitored with an online gas chromatograph equipped with both a thermal conductivity detector (TCD) and flame ionization detector (FID). In terms of kinetics studies, to keep the reaction in the kinetic regime, the conversion of CH_4 on these catalysts must be lower than 15%.[35] Thus, a temperature range of 440°C-520°C was chosen for the kinetic studies of these catalysts to keep conversion lower than 15%. In terms of catalytic performance on bare CeO_2 nanorods, it was examined under the exact same catalytic condition as Rh_1/CeO_2. The equations used for the activity measure are summarized as below.

$$(1)\quad \boldsymbol{Conversion(CH_4)} = \frac{[\boldsymbol{CH_4}]_{in} - [\boldsymbol{CH_4}]_{out}}{[\boldsymbol{CH_4}]_{in}} \times \mathbf{100}\%$$

$$(2)\quad \boldsymbol{Selectivity\ (CO)} = \frac{[\boldsymbol{CO}]_{out}}{[\boldsymbol{CH_4}]_{in}} \times \mathbf{100}\%$$

$$(3)\quad \boldsymbol{Selectivity\ (H_2)} = \frac{\frac{1}{2} \times [\boldsymbol{H_2}]_{out}}{[\boldsymbol{CH_4}]_{in}} \times \mathbf{100}\%$$

In equation (1)-(3), the $[\boldsymbol{CH_4}]_{in}$ and $[\boldsymbol{CH_4}]_{out}$is the CH_4 concentration in the inlet and outlet of the reactor, respectively. The $[\boldsymbol{CO}]_{out}$ and $[\boldsymbol{H_2}]_{out}$ is the CO and H_2 concentration at the outlet of the reactor.

$$(4)\quad \boldsymbol{TOF} = \frac{\boldsymbol{F \times X \times S \times \xi \times MW(Rh)}}{\boldsymbol{m_{catalyst} \times x}\%}$$

In equation (4), $\boldsymbol{F}$ is the molar flow rate of the CH_4 (mol/s), $\boldsymbol{X}$ is the conversion of CH_4, $\boldsymbol{S}$ is the selectivity for producing CO or H_2, $\boldsymbol{\xi}$ is 1 and 2 for CO and H_2, respectively. $\boldsymbol{MW(Rh)}$ is the molar mass of Rh element, $\boldsymbol{m_{catalyst}}$ is the mass of the catalyst used for kinetics studies, $\boldsymbol{x}\%$ is the mass percentage of Rh in the catalyst.

3. Results and discussion

3.1 Structure and characterization of Rh_1/CeO_2 catalyst

The 0.20wt%Rh/CeO_2 catalyst was prepared as described in experimental section. The prepared Rh/CeO_2 catalyst was examined for its physical and chemical properties. First of all, the authentic Rh content in the catalyst was 0.17 wt% measured by ICP-AES. This value is consistent with the nominal value of 0.20wt%. Thus, it is refereed as 0.20wt%Rh/CeO_2 catalyst in this work. The XRD analysis of the used catalyst 0.20wt%Rh/CeO_2 was performed to investigate whether Rh or Rh_2O_3 nanocrystals on the CeO_2 could have been formed in the preparation of this catalyst or during catalysis. The X-ray irradiation of Mo Kα line was used as the diffraction source. As shown in Figure 1a is the diffraction patterns of the 0.20wt%Rh/CeO_2 catalyst upon used for catalysis at 700°C. The used 0.20wt%Rh/CeO_2 exhibits the same XRD pattern as the primitive CeO_2 which belongs to cubic crystal system and *m3m* point group. The diffraction peaks observed at 28.3°, 32.8°, 47.0°, 55.8°, 58.5°, 68.7°, 75.8°, 78.2°, 87.4°, and 94.2° in Figure 1a match exactly with (111), (200), (220), (311), (222), (400), (331), (420), (422) and (333) crystal planes of CeO_2 respectively.[35, 42] Notably, there is lack of diffraction peaks of Rh metal or Rh_2O_3 in Figure 1a; it at least suggests neither Rh metal nor Rh_2O_3 nanocrystals with a size of ≥ 2 nm was formed during high temperature catalysis since XRD is only sensitive enough for identifying potential formation of rhodium metal or rhodium oxide nanoparticles with a size of ≥2 nm.

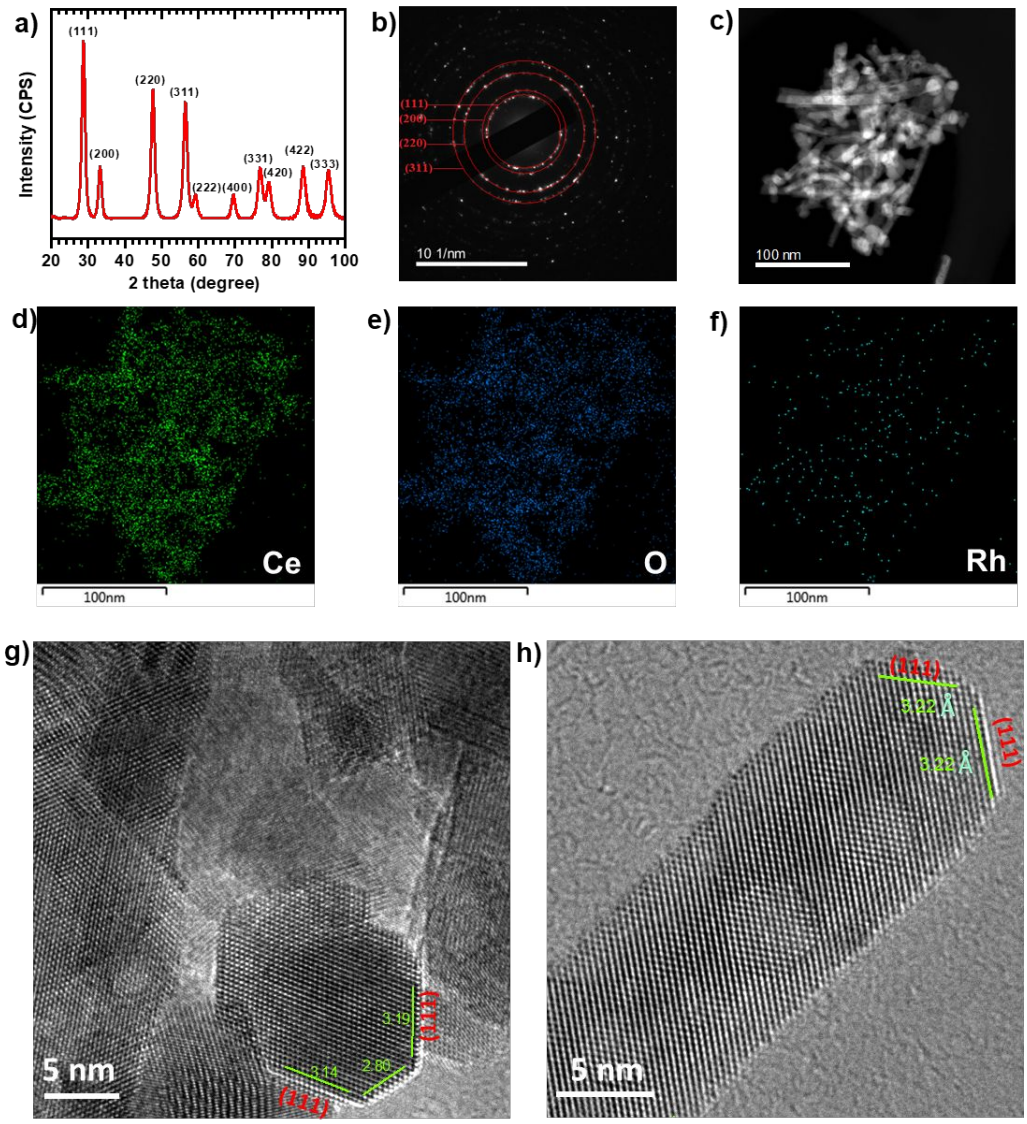

Figure 1. XRD and TEM studies of 0.20wt% Rh/CeO_2 catalyst after POM at 700°C. (a) XRD pattern. (b) SAED pattern, (c) STEM images, and (d-f) EDX mappings of Ce, O and Rh elements for the same region of (c). (g) and (h) HRTEM images. Interplanar distances were marked in (g) and (h).

The morphology of 0.20wt%Rh/CeO_2 catalyst nanoparticles was characterized with HRTEM (Figure 1b-f). The crystallization of CeO_2 of 0.20wt%Rh/CeO_2 used for catalysis was confirmed by the Selected Area Electron Diffraction (SEAD) pattern (Figure 1b). The diffraction rings of the lattice fringes of CeO_2 of the used catalyst were identified. The element dispersion of the catalyst is demonstrated in Figure 1c-f. The Ce, O, and Rh are uniformly dispersed in the catalyst. Nevertheless, TEM characterization suggests that (111) with an interplanar distance of 0.32 nm is the predominantly exposed face of CeO_2 of the used catalyst 0.20wt%Rh/CeO_2 as shown in Figures 1g-h. The pulsed CO chemisorption was performed for determining the dispersion of Rh atoms on surface of the catalyst 0.20wt%Rh/CeO_2 for aiding the exploration of dispersion of Rh atoms. Notably, the chemisorption measurement showed that the dispersion of Rh atoms on 0.20wt%Rh/CeO_2 is as high as 92.8%. The high dispersion of loaded Rh atoms on CeO_2 of 0.20wt%Rh/CeO_2 shows that 92.8% of these Rh atoms introduced to CeO_2 nanorods were dispersed on *surface* of CeO_2 nanorods of the 0.20wt%Rh/CeO_2 catalyst instead of subsurface or bulk of the support CeO_2. More importantly, it further suggests that majority of Rh atoms are singly dispersed on surface of the CeO_2 support. The high single dispersion of Rh atoms was consistent with the coordination environment of Rh atoms identified through EXAFS and DRIFT studies.

3.2 Catalytic performance and kinetics studies

The catalytic activity for partial oxidation of methane was evaluated in the fixed-bed tubular reactor. The main products of partial oxidation of methane are CO and H_2. The observed byproducts are CO_2 and H_2O which were formed from complete oxidation of CH_4. The conversion of CH_4 and selectivity for H_2 and CO through POM on the Rh_1/CeO_2 catalyst as a function of temperature in 300°C-700°C are plotted in Figure 2a. To confirm the role of singly dispersed Rh atoms, catalytic activity and selectivity for POM on bare CeO_2 nanorods were measured

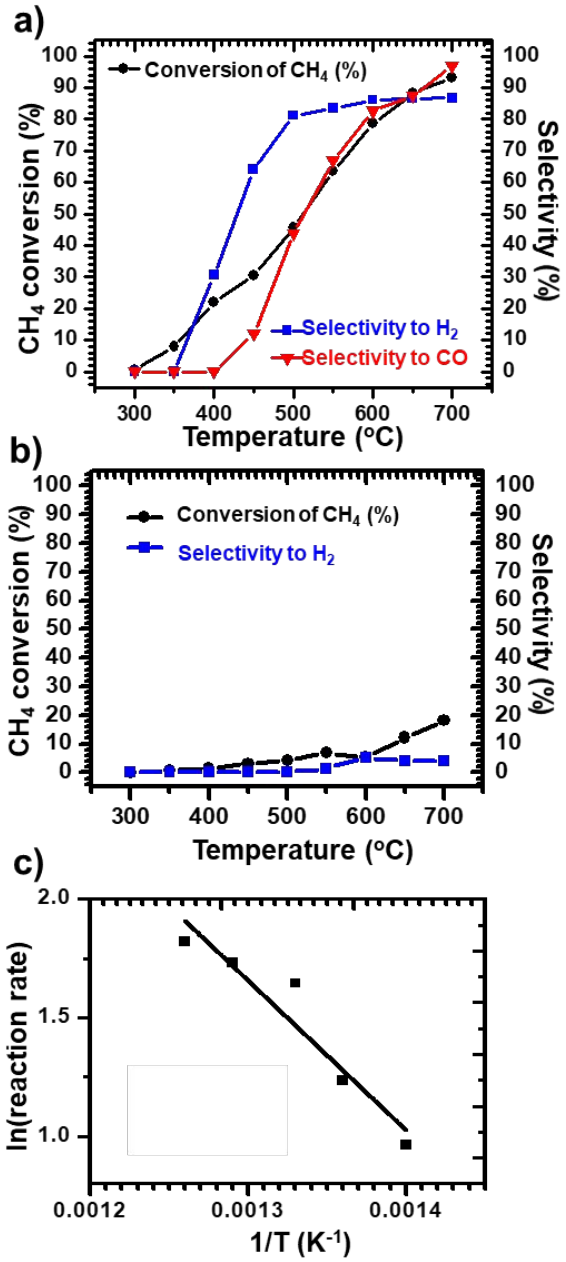

Figure 2. Catalytic performances of Rh_1/CeO_2 and bare CeO_2 (reference) for partial oxidation of methane. Conversion of CH_4 and selectivities for production of CO and H_2 as a function of temperature on (**a**) Rh_1/CeO_2 and (**b**) pure CeO_2 nanorods. **(c)** Arrhenius plot of ln (reaction rate for production of CO) as a function of 1/T (T in Kelvin).

under the same catalytic condition as that used for Rh_1/CeO_2. As shown in Figure 2b, no measurable conversion of CH_4 on 30 mg bare CeO_2 nanorods was observed up to 500°C. Even at 550°C and 700°C, only 7% and 18% CH_4 were converted on the 30 mg bare CeO_2 nanorods, respectively. Notably, the selectivity for production of H_2 on pure CeO_2 nanorods is extremely low, only 2% at 550°C and 5% at 700°C (Figure 2b); the selectivity for production of CO on 30 mg of bare CeO_2 nanorods at 300-700°C is even zero. The quite low activity in transforming CH_4 and the extremely low selectivity for production of CO and H_2 on bare CeO_2 shows that bare CeO_2 is nearly not active for POM. Sharply different from 30 mg bare CeO_2 nanorods, 0.20wt%Rh/CeO_2 exhibits high activity in POM and high selectivity for producing CO and H_2. Yields of H_2 and CO at 650°C on 30 mg 0.20wt%Rh/CeO_2 catalyst are 79% and 79%, respectively; the yields for H_2 and CO are 83% and 91% at 700°C, respectively. This distinct difference in catalytic performance of POM between pure CeO_2 and 0.20wt%Rh/CeO_2 confirmed the significant role of singly dispersed Rh_1 atoms in catalyzing POM.

Kinetic studies were conducted for evaluating the apparent activation energy of POM on Rh_1/CeO_2. To keep conversions of CH_4 lower than 15%, the kinetics were performed in the temperature range of 440°C-520°C instead of 600°C-700°C. Reaction rate and apparent activation energy for POM on this single-atom catalyst were derived from the Arrhenius plot of Rh_1/CeO_2 obtained from this kinetics study (Figure 2c). The apparent activation energy for POM on Rh_1/CeO_2 evaluated from this Arrhenius plot is 52.4 kJ/mol. By using the yields of CO or H_2 measured under kinetics control regime, TOFs for producing of CO and H_2 at 520°C were calculated. The TOF was calculated with equation (4) in Section 2.3. They are 1.41 CO and 2.81 H_2 molecules per Rh_1 site *per second* at 520°C, respectively, suggesting an outstanding catalytic performance for partial oxidation of methane.

3.3 Single dispersion of Rh atoms anchored on CeO2 surface during catalysis

3.3.1 In-situ X-ray absorption spectroscopy studies on the electronic and coordination state of Rh atoms

The XANES and EXAFS studies of the 0.20wt%Rh/CeO_2 catalyst after catalysis at different temperatures were conducted under an in-situ characterization mode as described in the experimental section. In these characterizations, catalysis was performed under the same catalytic condition (600°C, 650°C, or 700°C) as the evaluation of catalytic performance in our catalysis lab and then the sample was immediately cooled to 150°C or so in the flowing mixture of reactants. The XANES overlaid spectra of Rh K-edge presented in Figure 3a suggest that the Rh atoms in the 0.20wt%Rh/CeO_2 during POM catalysis at 600°C, 650°C and 700°C are at cationic state as shown by the edge position of Rh K-edge appeared at an energy higher than that of the reference sample, Rh metal foil. The cationic state of Rh atoms of 0.20wt%Rh/CeO_2 under catalytic conditions was further supported by the similarity between the edge position of Rh K edge of the reference sample, Rh_2O_3 and that of the 0.20wt%Rh/CeO_2 during POM catalysis. The high dispersion measured with the pulsed CO chemisorption and the cationic state of Rh atoms observed with XANES during catalysis suggest that Rh atoms anchored on CeO_2 of 0.20wt%Rh/CeO_2 during catalysis are singly dispersed cations, which is supported by the following EXAFS analysis.

The fitting of the r-space spectrum of Rh K-edge of the as-prepared 0.20wt%Rh/CeO_2 before catalysis shows that a Rh atom coordinates with 6.7 oxygen atoms on average (entry 1 in **Table 1**). Notably, no contribution of Rh-Rh scattering path was

needed in fitting the experimental r-space spectrum of the as-prepared 0.20wt%Rh/CeO_2, suggesting no Rh metal nanoparticles were formed on the catalyst. Thus, both XANES and EXAFS studies of 0.20wt% Rh/CeO_2 catalyst before catalysis show that no Rh metal nanoparticle was formed on the as-prepared 0.20wt% Rh/CeO_2.

these interatomic distances and coordination numbers listed in entries 2-4 in Table 1. This assumption is consistent with assignment of coordination environment of Rh atom in Rh_1/ZSM-5 (Figure 3e).[43] As shown in Figure 3f, the Rh-O-Rh of Rh_2O_3 nanoparticles appears at 2.68 Å before a phase correction. However, in Figures 3b-and 3d they are at 2.45 Å

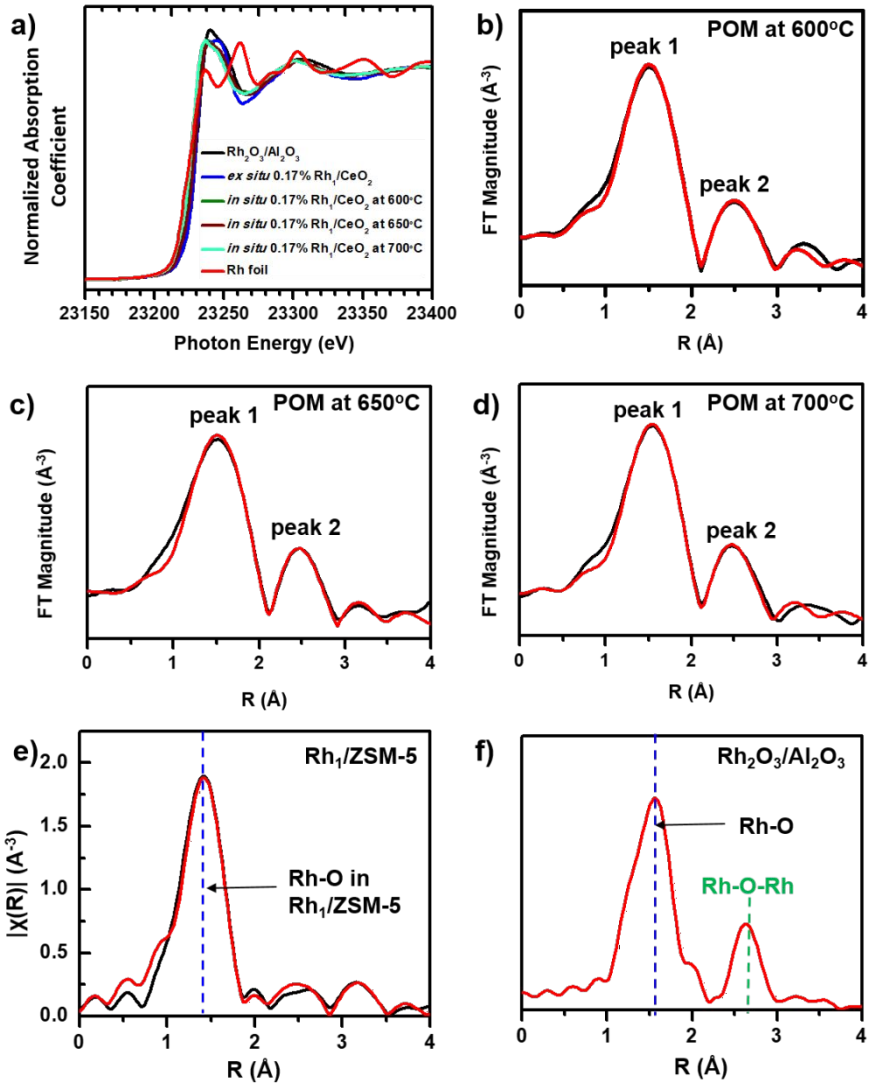

Figure 3. *in-situ* XAS studies of Rh K edge of 0.20wt%Rh/CeO_2 catalyst and r-space spectra of Rh K-edge of reference samples (Rh_1/ZSM-5 and Rh_2O_3/Al_2O_3). (a) XANES spectra of 0.20wt% Rh/CeO_2 catalyst (ex-situ), of 0.20wt%Rh/CeO_2 during catalysis at 600°C (green), 650°C (brown) and 700°C (blue) and of reference samples, Rh_2O_3/Al_2O_3 and Rh foil. (b-d) Fourier-transformed r-space fitting of Rh K-edge of 0.20wt% Rh/CeO_2 catalyst obtained from in situ study mode at 600°C (green), 650°C (brown) and 700°C (blue). In the in-situ study mode, the catalyst was heated to a catalysis temperature such as 700°C and remained at the temperature for 1 hr and then cooled down to 100-150°C in the reactant gases and remained at 100-150°C in the reactant gases where raw data of EXAFS studies were collected. (e) r-space spectrum of Rh K-edge of Rh_1/ZSM-5. (f) r-space spectra of Rh K-edge of Rh_2O_3 nanoparticles supported on TiO_2. All FT-EXAFS spectra are demonstrated without phase correction.

The r-space spectra of Rh K-edge of 0.20wt%Rh/CeO_2 collected under in situ catalytic conditions corresponding to catalysis at 600°C, 650°C and 700°C were presented in black lines in Figure 3b, 3c and 3d, respectively. Notably, the distances cited in the text and table are always values after a phase correction of data analysis except a specific note. The 1st shells of these *r*-space spectra of Rh K-edge were fitted to Rh-O with before a phase correction. In fact, the peak 2 is assigned to Rh-O-Ce instead of Rh-O-Rh. The fitting parameters for the r-space spectra of Rh K-edge collected under in situ catalytic conditions in entry 2-4 in Table 1 suggest that the Rh atoms bonded with surface lattice oxygen atoms and maintained their single dispersion under catalysis conditions at 600-700°C.

3.3.2 DRIFT study by using CO as probe molecule

Diffuse reflectance infrared Fourier transform spectroscopy of adsorbed CO (DRIFT-CO) was used for aiding the identification of dispersion of noble metal atoms, particularly Rh on transition meal oxide although it alone does not give a conclusive result.[34, 44-46] Here it is used for aiding identification of the dispersion of these anchored Rh atoms on CeO_2 of the used catalysts upon POM. The single dispersion of Rh atoms on CeO_2 surface suggested by EXAFS studies was supported with the DRIFT-CO experiment. The DRIFT-CO experiments were performed on a bare CeO_2 and the 0.20wt%Rh/CeO_2 catalysts used for POM at 500°C, 650°C or 700°C. Based on literature,[47-50] ν(CO) frequencies of free CO molecules in gas phase, CO adsorbed in μ_1 mode where a CO molecule adsorbs on top of a metal atom, CO adsorbed in μ_2 mode where a CO molecule bridges on two metal atoms, and CO adsorbed in μ_3 mode where a CO molecule bridges on three metal atoms, are 2143 cm^{-1}, 2120-1850 cm^{-1}, 1850-1750 cm^{-1} and 1730-1620 cm^{-1}, respectively. μ_1 mode is also called a terminal binding mode in which a CO molecule is adsorbed on top of a metal atom; it is the binding configuration of a single CO molecule bonded on a metal atom referred to atop in surface science or the germinal-dicarbonyl binding configuration; In the case of the germinal-dicarbonyl binding configuration, two CO molecules are simultaneously bound to a metal atom; this binding configuration leads to the presence of symmetric and asymmetric stretching peaks of the C≡O bond. Thus, for a germinal-dicarbonyl binding, simultaneous observation of two stretching peaks of C≡O bond are expected. For a surface consisting of continuously packed metal atoms in terms of surface of a metal nanoparticle or single crystal, CO molecules are adsorbed through μ_2 or/and μ_3 binding modes instead of μ_1. μ_2 or/and μ_3 mode is typically observed on surface consisting of continuously packed metal atoms in terms of surface of a metal nanocrystal or a macroscopic metal single crystal.[47-50] Whether ν(CO) bands of μ_1 mode is observed or not is an approach for deducing whether metal cations are singly dispersed or not. As described in the following paragraphs, the appearance of only atop and/or germinal dicarbonyl bands but not μ_2 or/and μ_3 in the DRIFT spectrum of the used catalyst suggests the presence of singly dispersed metal atoms on surface of a catalyst.

Table 1. The parameters used in fitting r-space spectra of the 0.20wt%Rh/CeO_2 catalyst before catalysis (ex-situ) (entry 1), obtained from in situ study of the catalyst at 600°C) (entry 2), 650°C (entry 3) and 700°C (entry 4).

Entry	Sample	Condition	Scattering Path	CN	Distance (Å)	σ^2 (Å^2)
1	0.20wt%Rh/CeO_2	*Ex-situ*	Rh–O	6.7±0.3	2.02±0.01	0.0033
2	0.20wt%Rh/CeO_2	*In-situ mode and catalysis at* 600°C	Rh–O	4.9±0.7	2.04±0.01	0.00436
			Rh–O–Ce	1.2±0.8	2.88±0.05	0.00301
3	0.20wt%Rh/CeO_2	*In-situ mode and catalysis at* 650°C	Rh–O	5.2±0.3	2.03±0.01	0.00464
			Rh–O–Ce	0.9±0.8	2.82±0.03	0.00542
4	0.20wt%Rh/CeO_2	*In-situ mode and catalysis at* 700°C	Rh–O	4.7±0.8	2.05±0.01	0.00320
			Rh–O–Ce	1.6±1.2	2.84±0.03	0.00329

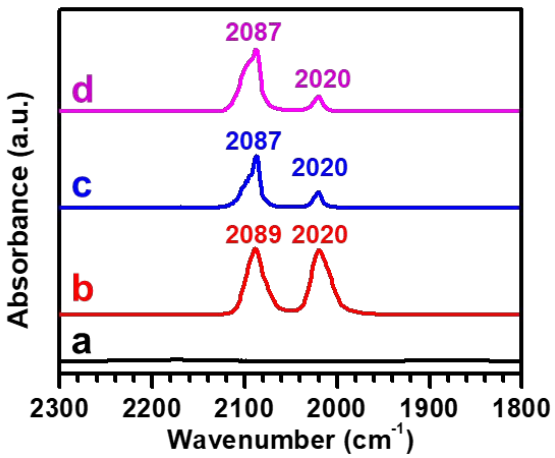

Figure 4. Diffuse reflectance infrared Fourier transformed (DRIFT) spectra of CO adsorbed on bare CeO_2 and used 0.20wt% Rh/CeO_2. a) pure CeO_2, and 0.20wt% Rh/CeO_2 catalyst after partial oxidation of methane at b) 500°C, c) 650°C, and d) 700°C.

Upon the blank experiment on bare CeO_2 (Figure 4a), catalysts 0.20wt%Rh/CeO_2 used for POM at 500°C, 650°C and 700°C were loaded separately. Figures 4b, 4c and 4d are the DRIFTS spectra of 0.20wt% Rh/CeO_2 collected after POM performed at 500°C, 650°C, and 700°C, respectively. The observed peak(s) of CO from the used 0.20wt%Rh/CeO_2 (Figures 4b-d) must result from chemisorption of CO molecules on Rh atoms of the used 0.20wt% Rh/CeO_2. In each of these spectra, there are always two bands at 2020 cm^{-1} and 2087-2089 cm^{-1}. The frequencies of the two bands are nearly the same as those of singly dispersed Rh atoms anchored on other oxide supports reported in literature,[47-50] suggesting that Rh atoms of the used catalyst are singly dispersed on CeO_2. In addition, the lack of vibrational signatures of μ_2 and μ_3 binding configurations of CO in Figure 4b-d suggests that Rh atoms of the used 0.20wt%Rh/CeO_2 are singly dispersed on CeO_2, consistent with the in situ studies of EXAFS (Figures 3b-d).

3.3.3 Ambient pressure XPS studies on the surface chemistry of Rh_1/CeO_2 catalyst

The surface of the catalyst 0.20wt%Rh/CeO_2 during POM was characterized by ambient pressure XPS (AP-XPS) during POM at

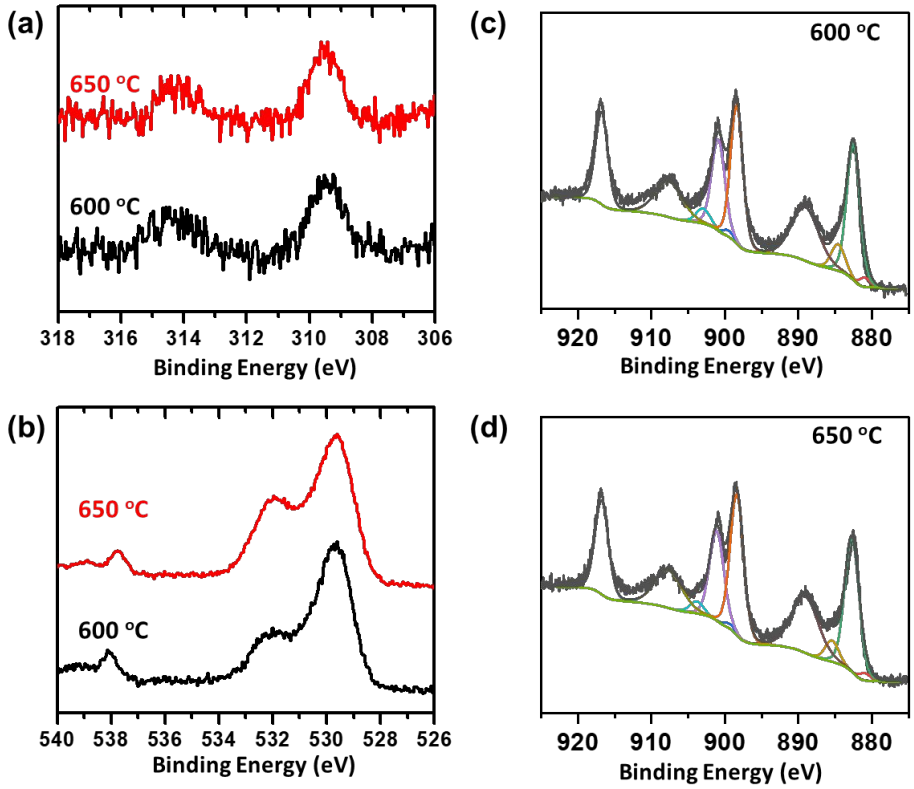

Figure 5. Near ambient pressure XPS studies of surface of catalyst Rh_1/CeO_2 (0.20wt%Rh/CeO_2) during catalysis in the mixture of 0.6 Torr CH_4 and 0.3 Torr O_2 at 600°C and 650°C. (a) Rh 3d, (b) O 1s, Ce 3d at (c) 600°C and (d) 650°C; existence of minor oxygen vacancies was confirmed by the observation of peak at 885.2 eV in (d).

600°C and 650°C.[36, 51] The photoelectron features of Rh *3d*, O *1s* and Ce *3d* of the 0.20wt%Rh/CeO_2 catalyst during catalysis at 600°C and 650°C are presented in Figure 5. It is well known that the spectrum of Ce *3d* of CeO_2 whose surface consists of both Ce^{4+} and Ce^{3+} is contributed from ten components of Ce^{4+} and Ce^{3+}.[7, 35, 42, 52-58] Six of them are characteristic satellite peaks of Ce^{4+} centered at 882.6 eV, 889.0 eV, 898.6 eV, 900.9 eV, 907.7 eV and 916.9 eV, respectively designated as v, v″, v‴, u, u″, and u‴, respectively;[37] the other four peaks centered at 880.6 eV, 885.2 eV, 899.2 eV, 904.0 eV labelled as v_o, v′, u_o, and u′, respectively are characteristic of Ce^{3+}; here u and v refer to the $3d_{3/2}$ and $3d_{5/2}$ of Ce atoms, respectively. Notably, the v′ peak of Ce^{3+} centered at 885.2 eV is considered as a characteristic feature of Ce^{3+} to indicate the portion of Ce^{3+} among Ce atoms since the v′ peak of Ce^{3+} appears at 885.2 eV since a deeper valley means a less portion of Ce^{3+}.[53, 59]

The relative intensity of these characteristic peaks of Ce^{3+} to the total intensity of all peaks represents density of oxygen vacancies (O_{vac}) in surface region of CeO_2 of the catalyst since the creation of an oxygen vacancy leaves two electrons to oxidize Ce^{4+} to Ce^{3+}.[37, 38] If there is lack of Ce^{3+} cations in surface region of CeO_2, the region between the v and v″ peaks of Ce^{4+} has deepest valley. Alternatively, along the increase of fraction of Ce^{3+} cations in surface region of CeO_2, the valley between the v and v″ peaks of Ce^{4+} is progressively filled up to become shallower. In fact, quantitative analysis through the deconvolution of Ce 3d spectra at 600°C and 650°C shows the atomic fractions of Ce^{3+} among cerium cations at 600°C and 650°C are 16.8% and 12.0% respectively (Figure 5c-d).

The binding energy of Rh *3d* of the catalyst 0.20wt%Rh/CeO_2 during catalysis at 600°C and 650°C is 309.1 eV, clearly showing the cationic nature of Rh atoms during catalysis (Figure 5a). The O *1s* spectra of the catalyst during catalysis were presented in Figure 5b. The O 1s peak centered at 529.6 eV can attribute to lattice oxygen atoms of CeO_2.[60-64] The O 1s shoulder at 532.0 eV can be attributed to non-stoichiometric oxygen atoms bonded to Ce^{3+} ions in oxygen vacancies or/and the adsorbed OH species on the catalyst although there have been debating on the two types of assignments.[7, 59, 65, 66] Quantitative analysis of the shoulder at 532.0 eV and the main peak at 529.6 eV suggests that the fractions of non-stoichiometric oxygen atoms binding to Ce^{3+} ions in the surface region of 0.20wt%Rh/CeO_2 during catalysis at 600°C and 650°C are about 26.7% and 34.8%, respectively. In addition, the O *1s* peaks at 537.4 eV is contributed from molecular O_2 which is one of the reactants. Similar O *1s* peaks of gas phase O_2 was observed due to the photoionization of electrons of reactant gas O_2 in literatures.[61, 67, 68] The observation of O 1s peak of gaseous O_2 (537.4 eV) by AP-XPS confirms that the Rh *3d*, Ce *3d* and O *1s* XPS peaks at 600°C and 650°C were definitely collected while the catalyst was in the gas phase mixture of reactants (CH_4 and O_2).

3.4 Insights on the POM on Rh_1/CeO_2 catalyst

Catalytically conversion of methane has been investigated for decades in terms of steam reforming (MSR), dry reforming of methane (DRM) and partial oxidation (POM). The conventional catalyst used for methane reforming is the supported metal nanoparticles on oxide, which suffers from deactivation due to coke formation of metal nanoparticles and sintering of metal nanoparticles to large particles.[8-10, 12] The recent theoretical chemistry investigation revealed that the continuous packed metallic metal-metal bond on the surface of Ni nanoparticles provides the opportunity to dissociate C-H bond of methane and further accumulation of C atoms to form coke.[69] Therefore, one strategy to design novel catalyst for methane reforming is by cracking the continuous packed metallic bond to form isolated sites on the oxide with strong metal-support interaction.[7, 25, 34, 35, 52] In other words, the single atom catalyst is a category of catalyst with great potential for methane reforming. However, the activation mechanism of methane over single-atom catalytic sites is distinct from that on supported metal nanoparticles due to the unique atomic structure of the catalyst.[20, 34, 35] As a result, the structure identification of the single atom sites is essential for the understanding of reaction mechanism.

As presented in this work, the Rh_1/CeO_2 catalyst has been successfully prepared and evaluated for POM reaction. The incorporation of Rh cations to the surface of ceria could promote the POM activity. Moreover, the singly dispersion of the Rh cations is confirmed by DRIFT-CO and chemisorption experiments. The electronic state and coordination state was studied by *in-situ* XAS and AP-XPS. The Rh remains cationic state during POM reaction. The CN (Rh-O) during POM is 4.7-5.2, which is under-saturated coordination. These low coordinated Rh cationic sites serve as sites for activating methane. Moreover, the surface oxygen vacancy is quantified by O1s spectra of AP-XPS, which plays significant role in the activation of molecule oxygen. The incorporation of singly dispersed Rh atom sites to CeO_2 surface with rich oxygen vacancies offers sites for activating methane and molecular O_2. Their intermediates can effectively couple on surface to form syngas. The single dispersion of cationic Rh atoms successfully avoided formation of coke which is a general challenge for supported metal nanoparticle catalyst.

4. Conclusions

In contrast to the endothermic nature of reforming CH_4 with H_2O or CO_2 to form syngas, the exothermic partial oxidation of CH_4 is a favorable process for production of syngas by utilization of CH_4 although a deep oxidation of CH_4 to form H_2O and CO_2 is a side reaction limiting catalytic selectivity toward production of syngas. Rh_1/CeO_2 was prepared with a modified deposition precipitation. At 350°C-700°C, it is highly active in production of CO and H_2 through POM with high selectivity. Yields of CO and H_2 on 30 mg of 0.20wt%Rh/CeO_2 at 700°C are 89% and 91%, respectively. Extensive in-situ/operando characterizations confirmed that Rh atoms are singly dispersed on surface of CeO_2 through coordinating with 4-5 surface lattice oxygen atoms during catalysis. This work demonstrated a significant modification by the anchored single transition metal atoms to these surface lattice oxygen atoms proximal to the anchoret Rh_1 atoms. Through introduction of Rh1 single atoms and modification of electronic state of surface lattice oxygen atoms, an efficient catalyst Rh_1/CeO_2 exhibiting high activity in POM and selectivity for producing syngas was developed.

Author Contributions

Adedamola A. Opalade: Investigation, Formal analysis, Writing - Original Draft. Yu Tang: Investigation, Formal analysis, Writing - Review & Editing, Franklin (Feng) Tao: Conceptualization, Writing - Review & Editing, Guidance of Science Development.

Conflicts of interest

There are no conflicts to declare.

Acknowledgements

This work was partially supported by Catalysis Science Program of the Chemical Sciences, Geosciences and Biosciences Division, Office of Basic Energy Sciences, Office of Science, U.S. Department of Energy under Grant DE-SC0014561. The authors highly appreciated J. Yang and S. House of University of Pittsburgh for their assistance in TEM characterization of catalysts, W. Huang group at Iowa State University for their assistance in DRIFT analysis of catalyst samples, and S. Tao and L. Tao for their significant amount of time input and effort in preparing this manuscript in the last two years.

Notes and references

1 J. Kang, Q.-Y. Fan, W. Zhou, Q. Zhang, S. He, L. Yue, Y. Tang, L. Nguyen, X. Yu, Y. You, H. Chang, X. Liu, L. Chen, Y. Liu, F. Tao, J. Cheng and Y. Wang, *Chem*, 2022, **8**, 1050-1066.

2 Y. Zhu, Y. Ye, S. Zhang, M. E. Leong and F. Tao, *Langmuir*, 2012, **28**, 8275-8280.

3 A. Y. Khodakov, W. Chu and P. Fongarland, *Chemical Reviews*, 2007, **107**, 1692-1744.

4 E. de Smit and B. M. Weckhuysen, *Chemical Society Reviews*, 2008, **37**, 2758-2781.

5 J. Wei, R. Yao, Y. Han, Q. Ge and J. Sun, *Chemical Society Reviews*, 2021, **50**, 10764-10805.

6 G. A. Olah, A. Goeppert, M. Czaun, T. Mathew, R. B. May and G. K. S. Prakash, *Journal of the American Chemical Society*, 2015, **137**, 8720-8729.

7 G. Yan, Y. Tang, Y. Li, Y. Li, L. Nguyen, T. Sakata, K. Higashi, F. F. Tao and P. Sautet, *Nature Catalysis*, 2022, **5**, 119-127.

8 A. Iulianelli, S. Liguori, J. Wilcox and A. Basile, *Catalysis Reviews-Science and Engineering*, 2016, **58**, 1-35.

9 M. Li, Z. Sun and Y. H. Hu, *Journal of Materials Chemistry A*, 2021, **9**, 12495-12520.

10 D. Pakhare and J. Spivey, *Chemical Society Reviews*, 2014, **43**, 7813-7837.

11 Y. H. Hu and E. Ruckenstein, in *Advances in Catalysis*, eds. B. C. Gates and H. Knozinger, 2004, vol. 48, pp. 297-345.

12 B. C. Enger, R. Lodeng and A. Holmen, *Applied Catalysis a-General*, 2008, **346**, 1-27.
13 Y. Kim, S. Kang, D. Kang, K. R. Lee, C. K. Song, J. Sung, J. S. Kim, H. Lee, J. Park and J. Yi, *Angewandte Chemie-International Edition*, 2021, **60**, 25411-25418.
14 P. Tomkins, M. Ranocchiari and J. A. van Bokhoven, *Accounts of Chemical Research*, 2017, **50**, 418-425.
15 Y. Tang, Y. Li and F. Tao, *Chemical Society Reviews*, 2022, **51**, 376-423.
16 E. D. German and M. Sheintuch, *Surface Science*, 2017, **656**, 126-139.
17 T. V. Choudhary and D. W. Goodman, *Journal of Molecular Catalysis a-Chemical*, 2000, **163**, 9-18.
18 F. Che, S. Ha and J.-S. McEwen, *Angewandte Chemie-International Edition*, 2017, **56**, 3557-3561.
19 S. Zhang, Y. Li, Z. Wang, Y. Tang, X. Huang, S. D. House, H. Huang, Y. Zhou, W. Shen, J. Yang, C. Wang, Y. Zhao, R. Schlögl, P. Hu and F. Tao, *ACS Catalysis*, 2021, **11**, 9837-9849.
20 V. Fung, F. Tao and D.-e. Jiang, *Physical Chemistry Chemical Physics*, 2018, **20**, 22909-22914.
21 R. M. Navarro, M. A. Pena and J. L. G. Fierro, *Chemical Reviews*, 2007, **107**, 3952-3991.
22 S. Cao, F. Tao, Y. Tang, Y. Li and J. Yu, *Chemical Society Reviews*, 2016, **45**, 4747-4765.
23 C. M. Ding, J. W. Wang, G. G. Ai, S. B. Liu, P. Liu, K. Zhang, Y. L. Han and X. S. Ma, *Fuel*, 2016, **175**, 1-12.
24 A. N. Pour and M. Mousavi, *International Journal of Hydrogen Energy*, 2015, **40**, 12985-12992.
25 H. Yang, R. Yu, Y. Fang, J. Yao, Y. Gan, J. Chen, H. Deng, X. Gao, X. Zong, J. Wang, L. Wu, L. Tan and Y. Tang, *Applied Surface Science*, 2022, **599**, 153863.
26 N. Lopez, T. V. W. Janssens, B. S. Clausen, Y. Xu, M. Mavrikakis, T. Bligaard and J. K. Norskov, *Journal of Catalysis*, 2004, **223**, 232-235.
27 E. Roduner, *Chemical Society Reviews*, 2006, **35**, 583-592.
28 P. Claus, A. Bruckner, C. Mohr and H. Hofmeister, *Journal of the American Chemical Society*, 2000, **122**, 11430-11439.
29 J. Liu, *Chemcatchem*, 2011, **3**, 934-948.
30 B. Yoon, H. Hakkinen, U. Landman, A. S. Worz, J. M. Antonietti, S. Abbet, K. Judai and U. Heiz, *Science*, 2005, **307**, 403-407.
31 G. A. Somorjai and J. Y. Park, *Chemical Society Reviews*, 2008, **37**, 2155-2162.
32 M. Crespo-Quesada, A. Yarulin, M. Jin, Y. Xia and L. Kiwi-Minsker, *Journal of the American Chemical Society*, 2011, **133**, 12787-12794.
33 R. Lang, X. Du, Y. Huang, X. Jiang, Q. Zhang, Y. Guo, K. Liu, B. Qiao, A. Wang and T. Zhang, *Chemical Reviews*, 2020, **120**, 11986-12043.
34 Y. Tang, V. Fung, X. Zhang, Y. Li, L. Nguyen, T. Sakata, K. Higashi, D.-e. Jiang and F. F. Tao, *Journal of the American Chemical Society*, 2021, **143**, 16566-16579.
35 Y. Tang, Y. Wei, Z. Wang, S. Zhang, Y. Li, L. Nguyen, Y. Li, Y. Zhou, W. Shen, F. F. Tao and P. Hu, *Journal of the American Chemical Society*, 2019, **141**, 7283-7293.
36 L. Nguyen and F. Tao, *Review of Scientific Instruments*, 2016, **87**, 064101
37 D. R. Mullins, S. H. Overbury and D. R. Huntley, *Surface Science*, 1998, **409**, 307-319.
38 M. Nolan, S. C. Parker and G. W. Watson, *Surface Science*, 2005, **595**, 223-232.
39 B. Ravel and M. Newville, *Journal of Synchrotron Radiation*, 2005, **12**, 537-541.
40 L. Nguyen and F. Tao, *Review of Scientific Instruments*, 2018, **89**, 024102.
41 L. Nguyen, Y. Tang, Y. Li, X. Zhang, D. Wang and F. Tao, *Review of Scientific Instruments*, 2018, **89**, 054103.
42 Y. Zhu, S. Zhang, J.-j. Shan, L. Nguyen, S. Zhan, X. Gu and F. Tao, *ACS Catalysis*, 2013, **3**, 2627-2639.
43 Y. Tang, Y. Li, V. Fung, D. Jiang, W. Huang, S. Zhang, Y. Iwasawa, T. Sakata, L. Nguyen, X. Zhang, A. I. Frenkel and F. Tao, *Nature Communications*, 2018, **9**, 1231.
44 S. Zhang, Y. Tang, L. Nguyen, Y.-F. Zhao, Z. Wu, T.-W. Goh, J. J. Liu, Y. Li, T. Zhu, W. Huang, A. I. Frenkel, J. Li and F. F. Tao, *ACS Catalysis*, 2018, **8**, 110-121.
45 J. C. Matsubu, S. Y. Zhang, L. DeRita, N. S. Marinkovic, J. G. G. Chen, G. W. Graham, X. Q. Pan and P. Christopher, *Nature Chemistry*, 2017, **9**, 120-127.
46 R. Lang, T. B. Li, D. Matsumura, S. Miao, Y. J. Ren, Y. T. Cui, Y. Tan, B. T. Qiao, L. Li, A. Q. Wang, X. D. Wang and T. Zhang, *Angewandte Chemie-International Edition*, 2016, **55**, 16054-16058.
47 J. C. Matsubu, V. N. Yang and P. Christopher, *Journal of the American Chemical Society*, 2015, **137**, 3076-3084.
48 Y. Kwon, T. Y. Kim, G. Kwon, J. Yi and H. Lee, *Journal of the American Chemical Society*, 2017, **139**, 17694-17699.
49 J. Yates Jr, T. Duncan, S. Worley and R. Vaughan, *The Journal of Chemical Physics*, 1979, **70**, 1219-1224.
50 C. Yang and C. W. Garl, *The Journal of Physical Chemistry*, 1957, **61**, 1504-1512.
51 L. Nguyen, F. F. Tao, Y. Tang, J. Doug and X.-J. Bao, *Chemical Reviews*, 2019, **119**, 6822-6905.
52 Y. Chen, B. deGlee, Y. Tang, Z. Wang, B. Zhao, Y. Wei, L. Zhang, S. Yoo, K. Pei, J. H. Kim, Y. Ding, P. Hu, F. F. Tao and M. Liu, *Nature Energy*, 2018, **3**, 1042-1050.
53 Z. Wu, Y. Cheng, F. Tao, L. Daemen, G. S. Foo, L. Nguyen, X. Zhang, A. Beste and A. J. Ramirez-Cuesta, *Journal of the American Chemical Society*, 2017, **139**, 9721-9727.
54 L. Ye, A. H. Mahadi, C. Saengruengrit, J. Qu, F. Xu, S. M. Fairclough, N. Young, P.-L. Ho, J. Shan, L. Nguyen, F. F. Tao, K. Tedsree and S. C. E. Tsang, *ACS Catalysis*, 2019, **9**, 5171-5177.
55 H. Sohn, G. Celik, S. Gunduz, D. Dogu, S. Zhang, J. Shan, F. F. Tao and U. S. Ozkan, *Catalysis Letters*, 2017, **147**, 2863-2876.
56 J. Li, Y. Tang, Y. Ma, Z. Zhang, F. Tao and Y. Qu, *ACS Applied Materials & Interfaces*, 2018, **10**, 38134-38140.
57 J. Dou, Y. Tang, L. Nie, C. M. Andolina, X. Zhang, S. House, Y. Li, J. Yang and F. Tao, *Catalysis Today*, 2018, **311**, 48-55.
58 X. Zhang, S. D. House, Y. Tang, L. Nguyen, Y. Li, A. A. Opalade, J. C. Yang, Z. Sun and F. F. Tao, *ACS Sustainable Chemistry & Engineering*, 2018, **6**, 6467-6477.
59 D. R. Mullins, *Surface Science Reports*, 2015, **70**, 42-85.
60 G. A. Carson, M. H. Nassir and M. A. Langell, *Journal of Vacuum Science & Technology a-Vacuum Surfaces and Films*, 1996, **14**, 1637-1642.
61 J. Zou, J. Gao and Y. Wang, *Journal of Photochemistry and Photobiology a-Chemistry*, 2009, **202**, 128-135.
62 J. T. Newberg, D. E. Starr, S. Yamamoto, S. Kaya, T. Kendelewicz, E. R. Mysak, S. Porsgaard, M. B. Salmeron, G. E. Brown, Jr., A. Nilsson and H. Bluhm, *Surface Science*, 2011, **605**, 89-94.
63 K. Li, S. Gao, Q. Wang, H. Xu, Z. Wang, B. Huang, Y. Dai and J. Lu, *ACS Applied Materials & Interfaces*, 2015, **7**, 9023-9030.
64 S. Yamamoto, T. Kendelewicz, J. T. Newberg, G. Ketteler, D. E. Starr, E. R. Mysak, K. J. Andersson, H. Ogasawara, H. Bluhm and M. Salmeron, *The Journal of Physical Chemistry C*, 2010, **114**, 2256-2266.
65 G. S. Herman, Y. J. Kim, S. A. Chambers and C. H. F. Peden, *Langmuir*, 1999, **15**, 3993-3997.
66 T. Hasegawa, S. M. F. Shahed, Y. Sainoo, A. Beniya, N. Isomura, Y.

Watanabe and T. Komeda, *Journal of Chemical Physics*, 2014, **140**, 044711.
67 B. Eren, C. Heine, H. Bluhm, G. A. Somorjai and M. Salmeron, *Journal of the American Chemical Society*, 2015, **137**, 11186-11190.
68 K. Yuan, J.-Q. Zhong, X. Zhou, L. Xu, S. L. Bergman, K. Wu, G. Q. Xu, S. L. Bernasek, H. X. Li and W. Chen, *ACS Catalysis*, 2016, **6**, 4330-4339.
69 Z. Wang, X. M. Cao, J. Zhu and P. Hu, *Journal of Catalysis*, 2014, **311**, 469-480.